PCCP

PAPER

View Article Online
View Journal | View Issue

Cite this: *Phys. Chem. Chem. Phys.*, 2014, **16**, 5129

Photoelectron spectroscopy of lithium and gold alloyed boron oxide clusters: charge transfer complexes, covalent gold, hyperhalogen, and dual three-center four-electron hyperbonds†

Wen-Juan Tian,[a] Hong-Guang Xu,[b] Xiang-Yu Kong,[bc] Qiang Chen,[a] Wei-Jun Zheng,*[bc] Hua-Jin Zhai*[a] and Si-Dian Li*[a]

Received 12th October 2013,
Accepted 16th January 2014

DOI: 10.1039/c3cp55362k

www.rsc.org/pccp

We report on the structural and electronic properties and chemical bonding in a series of lithium and gold alloyed boron oxide clusters: $B_2O_3^-$, $LiB_2O_3^-$, $AuB_2O_3^-$, and $LiAuB_2O_3^-$. The clusters have been produced by laser vaporization and characterized using photoelectron spectroscopy, in combination with the Coalescence Kick and Basin Hopping global-minimum searches and density-functional theory and molecular orbital theory calculations. Electron affinities of B_2O_3, LiB_2O_3, AuB_2O_3, and $LiAuB_2O_3$ neutral clusters are measured to be 1.45 ± 0.08, 4.25 ± 0.08, 6.05 ± 0.08, and 2.40 ± 0.08 eV, respectively. The experimental and computational data allow the cluster structures to be established for the anions as well as their neutrals. While $B_2O_3^-$ (C_{2v}) is bent, the three alloy clusters, $LiB_2O_3^-$ ($C_{\infty v}$), $AuB_2O_3^-$ (C_s), and $LiAuB_2O_3^-$ ($C_{\infty v}$), adopt linear or quasi-linear geometries with a metal center inserted between BO and OBO subunits, featuring charge transfer complexes, covalent gold, hyperhalogen, and dual three-center four-electron (3c-4e) π hyperbonds. The current results suggest the possibility of altering and fine-tuning the properties of boron oxides *via* alloying, which may lead to markedly different electronic structures and chemical reactivities. The LiB_2O_3 cluster belongs to the class of oxidizing agents called superhalogens, whereas AuB_2O_3 is a hyperhalogen species. Dual 3c-4e π hyperbonds represent a critical bonding element in boron oxides and are considered to be the root of delocalized bonding and aromaticity therein.

1. Introduction

Boron has a high affinity for oxygen and the study of combustion of boron and boranes has been persistently pursued over the past 50 years, aiming at the development of energetic boron-based propellants.[1] However, a molecular-level understanding of boron oxides has remained limited. A recent surge of research activities has focused on electronic and structural properties and chemical bonding in boron oxide clusters using a combined experimental and computational approach, leading to the emergence of a subfield of the so-called "boronyl chemistry",[2–11] where the boronyl group with a robust B≡O triple bond[9,10] governs the structures and bonding in the boron oxide systems. The boronyl chemistry is anticipated to parallel those of CN and CN^-/CO, which are isovalent to BO and BO^-, respectively.

To date, studies on boron oxide clusters have been generally dealing with relatively boron-rich species, in which boronyl groups occupy either terminal or bridging positions. The ratio of B *versus* O offers an additional degree of freedom to alter the properties of the boron oxide clusters and to "design" novel molecules.[2,11] Efforts along this line led to the recent discovery of the perfectly planar boronyl boroxine D_{3h} B_6O_6 cluster,[11] a new member of the inorganic benzene family and an exact boron oxide analog of boroxine and benzene.

The B_2O_3 cluster is the smallest stoichiometric boron oxide species in which B and O assume their favorite +3 and −2 formal oxidation states, respectively. Such species should be stable and chemically inert. Early matrix infrared (IR) spectroscopy studies suggested a "V" structure with an O apex

[a] *Nanocluster Laboratory, Institute of Molecular Science, Shanxi University, Taiyuan 030006, China. E-mail: hj.zhai@sxu.edu.cn, lisidian@sxu.edu.cn*
[b] *State Key Laboratory of Molecular Reaction Dynamics, Institute of Chemistry, Chinese Academy of Sciences, Beijing 100190, China. E-mail: zhengwj@iccas.ac.cn*
[c] *University of Chinese Academy of Sciences, Beijing 100049, China*

† Electronic supplementary information (ESI) available: Complete citation of ref. 30. Photoelectron spectrum of $B_2O_3^-$ recorded at 266 nm photon energy; alternative optimized structures for $B_2O_3^-$, $LiB_2O_3^-$, $AuB_2O_3^-$, and $LiAuB_2O_3^-$ at the MPW1PW91/6-311+G(d,p) level; pictures of canonical molecular orbitals, natural charge distribution, and NRT analyses for the global-minimum anion structures; calculated ADEs and VDEs for the second lowest-lying isomers of $B_2O_3^-$, $LiB_2O_3^-$, and $AuB_2O_3^-$. See DOI: 10.1039/c3cp55362k

attached by two BO groups, although the exact ∠BOB bond angle is uncertain.[12–14] The ionization potential of B_2O_3 was estimated to be ~13.3 eV based on thermodynamic data.[15] However, little is known about its electronic excited states, as well as its electron affinity (EA). In the present contribution, we report a combined photoelectron spectroscopy (PES) and density-functional theory (DFT) and molecular orbital (MO) theory study on the electronic and structural properties and chemical bonding in a series of lithium and gold alloyed boron oxide clusters: $B_2O_3^-$, $LiB_2O_3^-$, $AuB_2O_3^-$, $LiAuB_2O_3^-$, and their neutrals. This series of clusters may be considered as simple, interesting model systems to show how metal centers can be incorporated into boron oxides and change their electronic, structural, and chemical properties, for which a molecular level understanding is still lacking. The EAs of B_2O_3, LiB_2O_3, AuB_2O_3, and $LiAuB_2O_3$ are measured from the PES spectra to be 1.45 ± 0.08, 4.25 ± 0.08, 6.05 ± 0.08, and 2.40 ± 0.08 eV, respectively. Structural searches using the Coalescence Kick (CK) and Basin Hopping (BH) methods led to establishment of the global-minimum cluster structures: $B_2O_3^-$ is bent, whereas the three $LiB_2O_3^-$, $AuB_2O_3^-$, and $LiAuB_2O_3^-$ alloy clusters are linear or quasi-linear with a metal center inserted between the BO and OBO subunits. Chemical bonding analyses reveal interesting features in these species, such as charge transfer complexes, covalent gold, hyperhalogen,[16] and three-center four-electron (3c-4e) π hyperbonds.[17] The results suggest the possibility of altering and fine-tuning the properties of the boron oxide systems *via* alloying. The LiB_2O_3 cluster is a new member of superhalogens,[18] whereas AuB_2O_3 belongs to the class of highly oxidizing agents called hyperhalogens.[16]

Determination of global-minimum cluster structures has remained a rather demanding task for computational chemistry. Despite their relatively small sizes, the current series of clusters are binary, ternary, and quaternary systems, which pose further complexity and challenge beyond imagination for manual structural searches. While novel molecules such as pentatomic BCONS,[19] periodane LiBeBCNOF,[20] and heavier periodane NaMgAlSiPSCl[21] were studied previously, these have remained pure computational fantasy. In the current work, we demonstrate that binary, ternary, and quaternary clusters can be definitively characterized using the powerful combination of experimental PES, unbiased computational structural searches, and DFT and MO theory calculations. The current approach may be applicable to other more sophisticated, *n*-ary systems of interest.

2. Experimental and theoretical methods

2.1. Photoelectron spectroscopy

The experiments were conducted on a home-built apparatus consisting of a laser vaporization cluster source, a time-of-flight (TOF) mass spectrometer, and a magnetic-bottle photoelectron spectrometer, which has been described elsewhere.[22] The lithium and gold alloyed boron oxide cluster anions were generated by laser ablation of a rotating and translating disk target ($Au/LiBO_2$ mole ratio 2 : 1) with the second harmonic of a nanosecond Nd:YAG laser (Continuum Surelite II-10). The typical laser power used in this work is about 10 mJ per pulse. Helium carrier gas with ~4 atm backing pressure was allowed to expand through a pulsed valve (General Valve Series 9) into the source to cool the formed clusters. Cluster anions were mass analyzed using the TOF mass spectrometer. The cluster anions of interest were selected using a mass gate, decelerated by a momentum decelerator, and crossed with the beam of an excimer laser (ArF: 193 nm) or an Nd:YAG laser (Continuum Surelite II-10; 532 and 266 nm) in the photodetachment region. Photoelectrons were analyzed using the magnetic-bottle photoelectron spectrometer. The resolution of the PES apparatus was about 40 meV at the electron kinetic energy of 1 eV. The PES spectra were calibrated using the spectra of Au^- obtained under similar conditions.

2.2. Computational methods

Structural searches were carried out using the CK[23] and BH[24] global-minimum search programs at the MPW1PW91/6-31G level for $B_2O_3^-$ and $LiB_2O_3^-$ and the MPW1PW91/LanL2DZ level for $AuB_2O_3^-$ and $LiAuB_2O_3^-$.[25,26] The first ten low-lying structures were then fully optimized at the MPW1PW91/6-311+G(d,p) level for $B_2O_3^-$ and $LiB_2O_3^-$ and the MPW1PW91/Au/Stuttgart/B,O,Li/6-311+G(d,p) level for $AuB_2O_3^-$ and $LiAuB_2O_3^-$. Relative energies for the top five isomers were further refined using the coupled cluster method with triple excitations (CCSD(T))[27] at the MPW1PW91 geometries (CCSD(T)//MPW1PW91). Relevant neutral structures were also optimized. Electronic binding energies (BEs) were calculated at the MPW1PW91/Au/Stuttgart/B,O,Li/6-311+G(d,p) and single-point CCSD(T) levels, as well as at the outer valence Green's function (OVGF) level.[28] Natural resonance theory (NRT) bond orders were obtained from natural bond orbital (NBO) analyses.[29] All calculations were performed using the Gaussian 09 package.[30]

3. Experimental results

The PES spectra of $B_2O_3^-$, $LiB_2O_3^-$, $AuB_2O_3^-$, and $LiAuB_2O_3^-$ clusters recorded at 193 nm are presented in Fig. 1. The adiabatic detachment energies (ADEs) and vertical detachment energies (VDEs) of these cluster anions as evaluated from the PES data are listed in Table 1. The 193 nm PES spectrum of the $B_2O_3^-$ cluster (Fig. 1a) has a low BE feature X centered at 2.22 eV and a high BE feature (A) above ~5.9 eV. Band X is very broad, probably due to the unresolved vibrational progressions of B_2O_3. We have also obtained the PES spectra of $B_2O_3^-$ with 532 and 266 nm photons, the latter being presented in Fig. S1 in the ESI.† However, the vibrational peaks cannot be resolved, probably due to the low frequencies of B–O–B bend modes[13] and the overlapping from multiple vibrational modes. Lacking a vibrational resolution, the ground-state ADE was determined by drawing a straight line along the leading edge of band X to cross the baseline and then adding the instrumental resolution

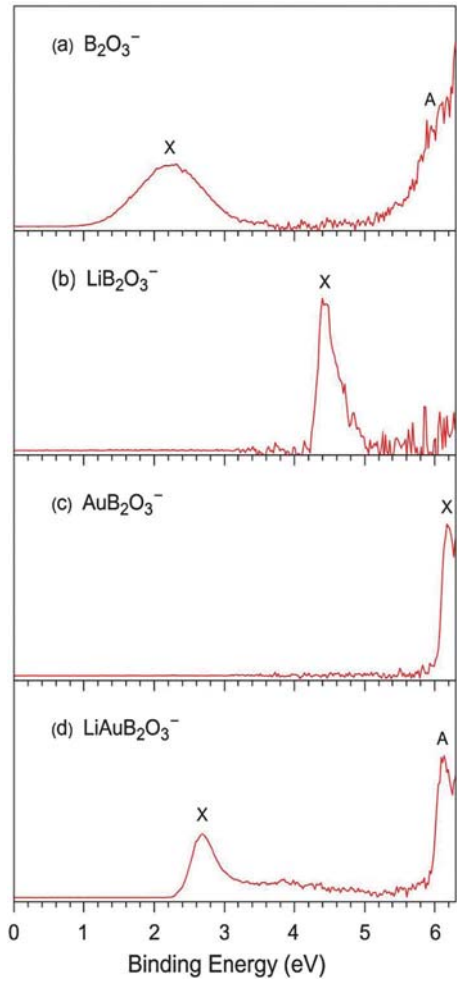

Fig. 1 Photoelectron spectra of (a) $B_2O_3^-$, (b) $LiB_2O_3^-$, (c) $AuB_2O_3^-$, and (d) $LiAuB_2O_3^-$ clusters recorded at 193 nm photon energy.

to the BE value at the crossing point. The ADE thus evaluated is 1.45 ± 0.08 eV; see Section 5 for further comments on this value.

The PES spectrum of $LiB_2O_3^-$ shows a single peak (X; Fig. 1b) centered at 4.43 eV, whose onset is substantially sharper. The spectrum of $AuB_2O_3^-$ (Fig. 1c) also has a sharp peak X with an extremely large VDE of 6.17 eV. The PES spectrum of $LiAuB_2O_3^-$ (Fig. 1d) consists of a low BE feature X centered at 2.68 eV and a high BE one (A) centered at 6.13 eV, as well as some low intensity electron signals between X and A bands, covering the BE range of 3.0–5.0 eV. The ground-state ADEs are estimated from the onset of band X to be 4.25, 6.05, and 2.40 eV for $LiB_2O_3^-$, $AuB_2O_3^-$ and $LiAuB_2O_3^-$, respectively, which are also the EAs of the corresponding neutral clusters.

4. Theoretical results

Our extensive CK and BH global-minimum searches have identified the low-lying cluster structures of $B_2O_3^-$, $LiB_2O_3^-$, $AuB_2O_3^-$, and $LiAuB_2O_3^-$, which are collected in Fig. S2–S5 in the ESI.† Their energetics was evaluated through full structural optimizations at the MPW1PW91/6-311+G(d,p) level, with that of the top five candidate structures being further refined at the single-point CCSD(T)//MPW1PW91/6-311+G(d,p) level. In short, four isomeric structures are within ~5 kcal mol^{-1} for $B_2O_3^-$: C_{2v} (**1**, $^2A_1$), C_s ($^2A'$), C_s ($^2A'$), and C_{2v} ($^2A_1$) (Fig. S2 in the ESI†). Two candidate structures, $C_{\infty v}$ (**2**, $^1\Sigma^+$) and $C_{\infty v}$ ($^1\Sigma^+$) (Fig. S3 in the ESI†), are found for $LiB_2O_3^-$, and two candidate structures for $AuB_2O_3^-$ as well: C_s (**3**, $^1A'$) and $C_{\infty v}$ ($^1\Sigma^+$) (Fig. S4 in the ESI†). For $LiAuB_2O_3^-$, the global minimum $C_{\infty v}$ (**4**, $^2\Sigma^+$) is well defined, with the nearest alternative structure being ~8 kcal mol^{-1} higher in energy (Fig. S5 in the ESI†). The anion global-minimum structures for the series and their corresponding neutral structures are presented in Fig. 2 along with the bond distances.

For the bent $B_2O_3^-$ (**1**) and linear or quasi-linear $LiB_2O_3^-$ (**2**), $AuB_2O_3^-$ (**3**), and $LiAuB_2O_3^-$ (**4**) anions, as well as their nearest competitive structures (Fig. S2–S5 in the ESI†), the BO and OBO subunits are apparent structural blocks, whose bond distances are 1.22–1.25 and 1.27/1.24 Å, respectively. The BO subunits can be faithfully assigned as boronyls with B≡O triple bonds.[9,10] The OBO subunits appear to be asymmetric, whose shorter distances (1.24 Å) are close to that of boronyl and the longer ones (1.27 Å) are only slightly longer than that of boronyl,

Table 1 Experimental adiabatic and vertical detachment energies (ADEs and VDEs) of $B_2O_3^-$, $LiB_2O_3^-$, $AuB_2O_3^-$, and $LiAuB_2O_3^-$ clusters, as compared to those calculated at the MPW1PW91/Au/Stuttgart/B,O,Li/6-311+G(d,p), single-point CCSD(T), and the outer valence Green's function (OVGF) levels[a]

			Exptl		Theor		
Species	Feature	Final state	ADE[b,c]	VDE[b]	ADE[d]	VDE[d]	VDE (OVGF)[e]
$B_2O_3^-$	X	$^1A_1$	1.45[f]	2.22	0.78 (*0.40*)	2.79 (*2.24*)	2.36
	A	$^3B_1$		~5.9		5.92 (*5.97*)	6.32
$LiB_2O_3^-$	X	$^2\Sigma^+$	4.25	4.43	4.25 (*4.19*)	4.39 (*4.30*)	4.38
$AuB_2O_3^-$	X	$^2A''$	6.05	6.17	6.01 (*6.16*)	6.04 (*6.16*)	6.50
$LiAuB_2O_3^-$	X	$^1\Sigma^+$	2.40	2.68	2.51 (*2.27*)	2.62 (*2.38*)	2.60
	A	$^3\Sigma^+$		6.13		6.08 (*5.77*)	6.49

[a] All energies are in eV. [b] Estimated experimental uncertainties: ±0.08 eV. [c] Electron affinity of the neutral cluster. [d] Ground-state ADEs and VDEs calculated at the MPW1PW91/Au/Stuttgart/B,O,Li/6-311+G(d,p) and single-point CCSD(T) (italic in the parentheses) levels. [e] Calculated at the OVGF/Au/Stuttgart/B,O,Li/6-311+G(d,p) level. [f] Due to the large anion-to-neutral geometric changes, the 0–0 transition may be negligibly small. The observed ADE should be considered as an upper limit of the true electron affinity.

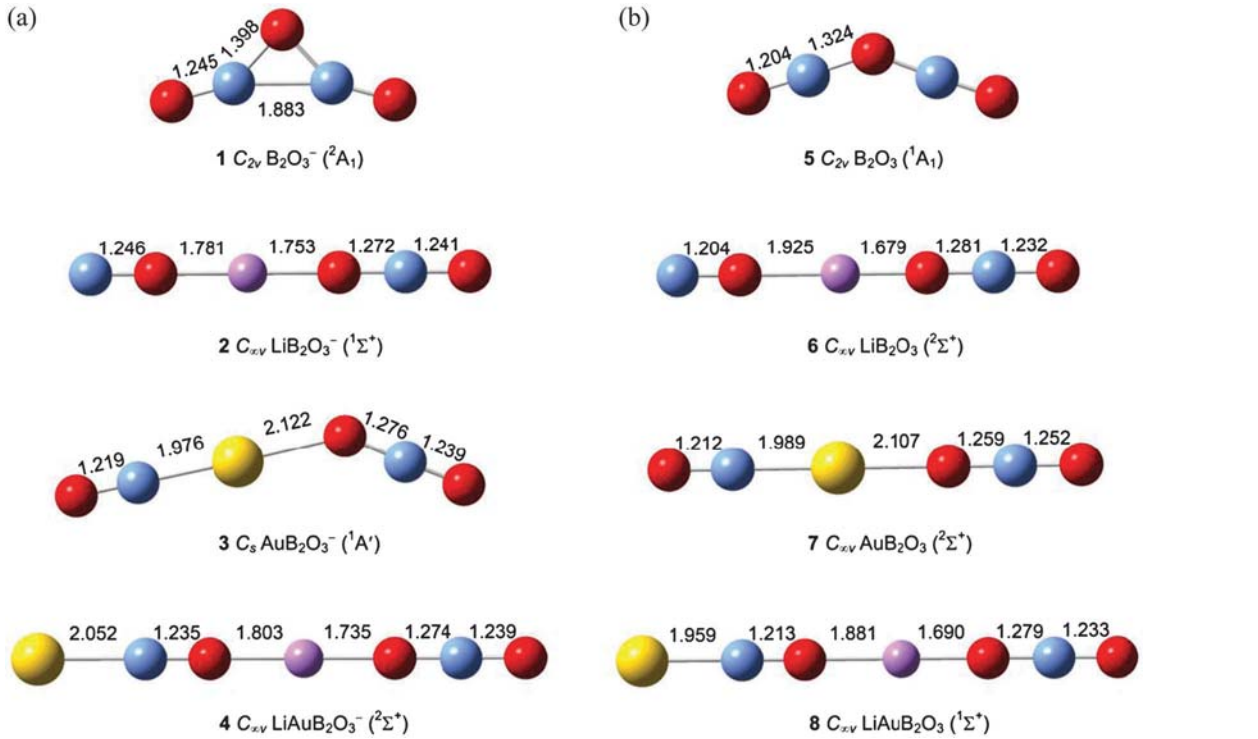

Fig. 2 (a) Global-minimum structures at the MPW1PW91/Au/Stuttgart/B,O,Li/6-311+G(d,p) level for $B_2O_3^-$ (**1**, C_{2v}, $^2A_1$), $LiB_2O_3^-$ (**2**, $C_{\infty v}$, $^1\Sigma^+$), $AuB_2O_3^-$ (**3**, C_s, $^1A'$), and $LiAuB_2O_3^-$ (**4**, $C_{\infty v}$, $^2\Sigma^+$) clusters. (b) Their corresponding neutral structures (**5–8**). Bond distances (in Å) are labeled. The structures are obtained *via* the Coalescence Kick and Basin Hopping global-minimum searches. B is in blue, O in red, Li in purple, and Au in yellow.

suggesting multiple bond characters. Furthermore, the B–Au distances of 1.98 and 2.05 Å in **3** and **4**, respectively, are typical single bonds.[6] In the neutral clusters **5–8**, the BO, OBO, and (O)BAu subunits retain similar bond distances. Structural changes occur from **1** to **5** upon electron removal, in which the BB distance elongates markedly from anion to neutral. Also, the neutral structure **7** is perfectly linear, in contrast to the bent anion structure **3**.

5. Comparison between experiment and theory

The experimental ADEs and VDEs of $B_2O_3^-$, $LiB_2O_3^-$, $AuB_2O_3^-$, and $LiAuB_2O_3^-$ clusters are compared with computational data at the MPW1PW91, single-point CCSD(T), and OVGF levels in Table 1, based on structures **1–4** *via* the CK and BH global-minimum searches. The MPW1PW91 calculations predict the ground-state VDEs to be within ~0.1 eV for $LiB_2O_3^-$, $AuB_2O_3^-$, and $LiAuB_2O_3^-$, but with a large error of ~0.6 eV for $B_2O_3^-$. In contrast, the calculated first VDEs at the OVGF level are within ~0.1 eV of the experimental data for $B_2O_3^-$, $LiB_2O_3^-$, and $LiAuB_2O_3^-$, although the predicted VDE for $AuB_2O_3^-$ is overestimated by ~0.3 eV. For the excited state bands, the MPW1PW91 data are also within ~0.1 eV of the experimental measurements for $B_2O_3^-$ and $LiAuB_2O_3^-$, whereas OVGF overestimates these by ~0.4 eV. Thus, MPW1PW91 appears to perform slightly better than OVGF for the current system.

In terms of the ground-state ADEs, that is, EAs of the neutral clusters, the MPW1PW91 calculations are in perfect agreement with experiment within ~0.1 eV for $LiB_2O_3^-$, $AuB_2O_3^-$, and $LiAuB_2O_3^-$. However, the predicted ADE for $B_2O_3^-$ (0.78 eV) is substantially lower than the measurements (1.45 ± 0.08 eV) with an error of ~0.7 eV, which is among the largest of all calculated values. We believe that this discrepancy is partly due to the large geometric changes from **1** to **5** upon electron detachment (Fig. 2), where the apex ∠BOB bond angle expands from 84.7° in **1** to 139.8° in **5**. As a consequence, the Franck–Condon overlapping for the 0–0 transition is negligibly small and the observed ADE should be considered as an upper limit of the true ADE. A typical, similar case was reported for an organic $C_8H_8^-$ anion by Lineberger and coworkers.[31]

The calculated ADEs and VDEs at the single-point CCSD(T) level (Table 1) are generally consistent with those at the MPW1PW91 level. Notable improvements include the ground-state VDE for $B_2O_3^-$, whose CCSD(T) value is in perfect agreement with experiment, being ~0.6 eV lower than that predicted at MPW1PW91. The CCSD(T) data further confirm that the observed ADE for $B_2O_3^-$ should be viewed as an upper limit for the true EA of the neutral. However, the calculated ground-state VDE for $LiAuB_2O_3^-$ at CCSD(T) deviates from the experimental data by ~0.3 eV, whereas that calculated at MPW1PW91 is in perfect agreement with the measurements. Overall, the agreement between experiment and theory is remarkable, lending considerable credence to the identified anion global-minimum structures **1–4** and their corresponding neutrals **5–8**. Additional

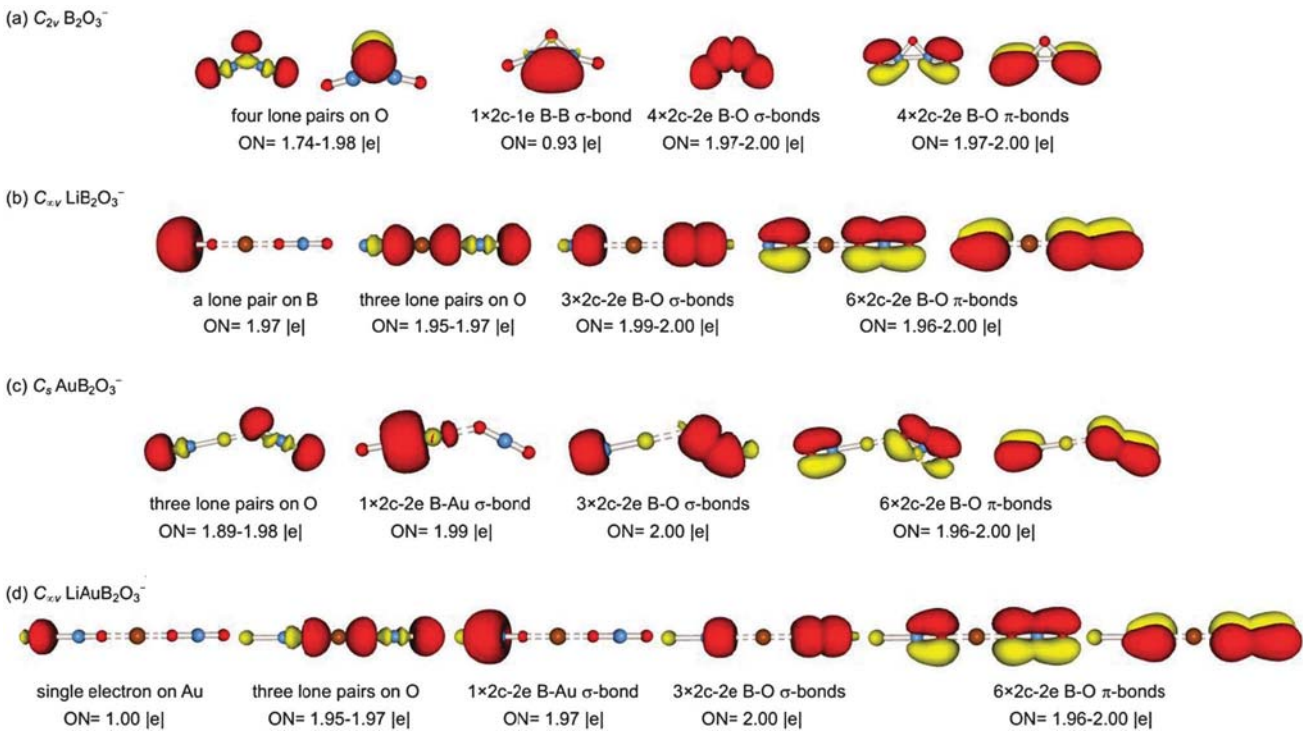

Fig. 3 AdNDP bonding patterns for the anion global-minimum structures: (a) $B_2O_3^-$ (**1**, C_{2v}, $^2A_1$), (b) $LiB_2O_3^-$ (**2**, $C_{\infty v}$, $^1\Sigma^+$), (c) $AuB_2O_3^-$ (**3**, C_s, $^1A'$), and (d) $LiAuB_2O_3^-$ (**4**, $C_{\infty v}$, $^2\Sigma^+$). The occupation numbers (ONs) are indicated.

computational data for the nearest low-lying isomers **1–3** are presented in Table S1 in the ESI.†[32]

6. Discussion

6.1. Lewis structures: charge transfer complexes *versus* covalent gold

As pointed out in Section 4, the BO, OBO, and (O)BAu structural blocks are readily identified in structures **1–8** (Fig. 2), featuring BO multiple bonds and BAu single bonds. The apex OB bonds in **1** and **5** are assigned to single bonds, whose distances range from 1.32 to 1.40 Å. In addition, the LiO bonding in **2**, **4**, **6**, and **8** is attributed to typical ionic bonds with little covalent contribution, whereas the AuO bonding in **3** and **7** appears to be relatively weak due to the large distances (~2.1 Å). Canonical MOs (Fig. S6–S9 in the ESI†) and adaptive natural density partitioning (AdNDP; Fig. 3)[33] analyses fully support the above assignments, which are further aided by the natural charge distributions (Fig. S10 in the ESI†) and the NRT bond orders (Tables S2–S5 in the ESI†) from the NBO analyses, allowing a thorough understanding of bonding in the system. The essence of chemical bonding in the global-minimum clusters **1–4** is summarized in the approximate Lewis structures, as depicted in Fig. 4.

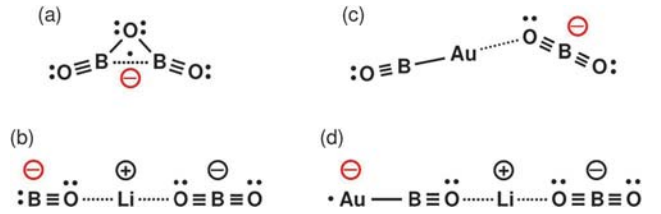

Fig. 4 Schematic Lewis presentation for the global-minimum structures: (a) $B_2O_3^-$ (**1**, C_{2v}, $^2A_1$), (b) $LiB_2O_3^-$ (**2**, $C_{\infty v}$, $^1\Sigma^+$), (c) $AuB_2O_3^-$ (**3**, C_s, $^1A'$), and (d) $LiAuB_2O_3^-$ (**4**, $C_{\infty v}$, $^2\Sigma^+$). Lone-pairs, single bonds, and triple bonds are labeled. The dashed line in (a) represents a two-center one-electron bond and the dotted lines in (b)–(d) indicate ionic interactions. Charge transfer from Li to OBO is shown in (b) and (d). The locations of the extra charge in anions are shown in red color according to their HOMOs.

The AdNDP method represents the electronic structure of a molecule in terms of *n*-center two-electron (*n*c-2e) bonds, with the *n* value ranging from one to the total number of atoms in the molecule, which recovers the classical Lewis bonding elements (lone-pairs and 2c-2e bonds) as well as nonclassical delocalized *n*c-2e bonds. Relative to the stoichiometric B_2O_3 cluster, the extra electron in $B_2O_3^-$ (**1**) occupies the 2c-1e BB σ bond (Fig. 3a). This results in substantial geometric changes between anion (**1**) and neutral (**5**), consistent with the broad PES band X observed experimentally (Fig. 1a). The two terminal B≡O triple bonds are perfectly recovered from AdNDP, as are the two BO single bonds associated with the O apex, which also possesses an O 2p lone-pair. Three O 2s lone-pairs are also identified, one on every O center.

In $LiB_2O_3^-$ (**2**) (Fig. 3b), AdNDP recovers the B≡O triple bond in the boronyl subunit. Threefold BO bonding is also revealed in the OBO subunit. A lone-pair is recovered on the terminal B and on every O center. There appears to be no covalent bonding associated with Li. NRT analysis indicates

that Li–O bonding between Li and OBO indeed shows no covalent character (Table S3 in the ESI†), which should be considered to be purely ionic. This leads to a charge transfer complex involving Li^+ and $[OBO]^-$, in which electrostatic stabilization plays a vital role. Note that the bonding in the OBO subunit is asymmetric with bond distances of 1.27 *versus* 1.24 Å (Fig. 2b), the exact nature of bonding of which will be discussed in Section 6.4.

The bonding in $AuB_2O_3^-$ (**3**) (Fig. 3c) features B≡O triple bonds, threefold BO bonds in the OBO subunit, and B–Au single bond, along with a lone-pair on each O center. It appears to consist of two relatively separated OBAu and $[OBO]^-$ subunits. Discernible Au···O covalent interaction exists in the MOs, although not recovered in the AdNDP analysis. The existence of typical B–Au σ bond in **3** (and in **4** as well) is an obvious reflection of covalent gold, which is a topic of current interest in Au chemistry.[34] Similar BO, OBO, and (O)BAu bonds and O lone-pairs are recovered in $LiAuB_2O_3^-$ (**4**) (Fig. 3d). An additional bonding element is an unpaired electron on Au. Again, AdNDP does not reveal O···Li···O bonding in **4**.

As shown in Tables S4 and S5 in the ESI,† the B–Au bonds are indeed highly covalent with a total NRT bond order of 1.00 (covalent: 0.79; ionic: 0.21) in **3** and 1.05 in **4** (covalent: 0.57; ionic: 0.48), in sharp contrast to the pure ionic Li–O bonds in **2** and **4**. Understandably, the covalent Au tends to bond with boronyl at the B site, whereas the ionic Li prefers the O site to maximize the electrostatic stabilization (Fig. 2). It may be argued that the quasi-linear geometry of **3** is also due to covalent gold.

6.2. Electronic structure trend: correlation with the frontier orbitals

The PES patterns change markedly along $B_2O_3^-$, $LiB_2O_3^-$, $AuB_2O_3^-$, and $LiAuB_2O_3^-$ clusters (Fig. 1), suggesting the possibilities of fine-tuning and drastically altering the electronic and chemical properties of boron oxides *via* alloying with Li and/or Au. For example, the PES spectrum of $B_2O_3^-$ (Fig. 1a) is characteristic of stable, closed-shell neutral cluster with a sizable energy gap of ~4.2 eV between the highest occupied MO (HOMO) and the lowest unoccupied MO (LUMO), as evaluated from the ADE difference between band X and band A. The corresponding HOMO–LUMO gap shrinks to ~3.6 eV in the spectrum of $LiAuB_2O_3^-$ (Fig. 1d). In contrast, $LiB_2O_3^-$ and $AuB_2O_3^-$ show remarkably enhanced VDE values, indicative of highly reactive and strongly oxidizing neutral species.

This electronic trend may be rationalized based on the change of the frontier MOs in the series (Fig. S6–S9 in the ESI†), which is also reflected in Fig. 4. The extra charge in **1** is B 2s/2p based, whereas those in **2–4** are located on the BO, OBO, and AuBO subunits, respectively. The natural charge distributions in **1–4** *versus* their neutrals **5–8** (Fig. S10 in the ESI†) are fully consistent with the nature of the above MOs. Indeed, the HOMOs in **2–4** are nearly identical to those in the BO^-, BO_2^-, and $AuBO^-$ clusters,[6,10] respectively. As a consequence, the first VDEs in **2–4** are 4.43, 6.17, and 2.68 eV, respectively (Table 1), correlating closely with those in the gas-phase BO^- (2.51 eV), BO_2^- (4.46 eV), and $AuBO^-$ (1.51 eV) clusters.[6,10] The covalent interaction with (O)BAu in **3** and the electrostatic interactions with $Li^+/[OBO]^-$ in **2** and **4** induce substantial stabilization for the HOMOs in **2–4**, by as much as ~1.9, ~1.7, and ~1.2 eV, respectively. Further exploration along this line should help design and produce novel complexes with even higher VDE or EA values.

6.3. AuB_2O_3: a hyperhalogen species

The PES spectrum of $AuB_2O_3^-$ (Fig. 1c) shows an extremely high EA of 6.05 ± 0.08 eV for the AuB_2O_3 neutral cluster (Table 1), which is among the highest of all gas-phase clusters and molecules.[35] Species with high EAs have been actively pursued as strong oxidizing agents over the past half century. Halogens represent the elements with the largest EAs (Cl: 3.61 eV) in the periodic table. Novel molecules called superhalogens, whose EAs far exceed those of the halogens, may be designed based on the formula proposed by Gutsev and Boldyrev.[18] The current LiB_2O_3 cluster, with an EA of 4.25 eV (Table 1), is a new member of the superhalogen family. Very recently, a concept of hyperhalogen was conceived by Jena and coworkers.[16] A hyperhalogen species, by definition, is composed of a metal core surrounded by superhalogen moieties and possesses an EA that is even larger than the corresponding superhalogen building blocks.

The simple BO_2 superhalogen (EA: 4.46 ± 0.03 eV)[10] has been widely explored as a candidate to build hyperhalogens[36–39] and a hyperhalogen with an EA as high as ~6.9 eV has been predicted.[39] Among hyperhalogen clusters experimentally characterized to date include $Cu(BO_2)_2$ and $Au(BO_2)_2$, whose EAs are 5.07 ± 0.08 and 5.7 ± 0.1 eV, respectively.[16,40] The current hyperhalogen AuB_2O_3 cluster possesses an EA of 6.05 ± 0.08 eV that is even greater than those of $Cu(BO_2)_2$ and $Au(BO_2)_2$, despite the fact that AuB_2O_3 possesses only one BO_2 superhalogen building block, as compared to two in $Cu(BO_2)_2$ and $Au(BO_2)_2$. We believe the reason for this difference is that the HOMOs in $Cu(BO_2)_2^-$ and $Au(BO_2)_2^-$ involve substantial Cu/Au characters. In contrast, the HOMO in $AuB_2O_3^-$ is primarily based on the BO_2 superhalogen subunit, which is further stabilized by an OBAu covalent subunit, as discussed above in Section 6.2. This understanding should guide the computational searches and designs of new hyperhalogen species.

6.4. On the dual 3c-4e π hyperbonds

One intriguing bonding feature in the system involves the OBO bonding in $LiB_2O_3^-$, $AuB_2O_3^-$, and $LiAuB_2O_3^-$ species (as well as in their neutrals), where the OBO subunit appears to be a robust structural block. In terms of BO distances, these are very close in all **2–4** and **6–8** species, which are similarly asymmetric: 1.26–1.28 *versus* 1.23–1.25 Å (Fig. 2). As a rough reference,[41] the double-bond covalent radii of B and O are recommended to be 0.78 and 0.57 Å, suggesting an upper limit of the B=O bond as 1.35 Å. Thus, the OBO bonding in the **2–4** and **6–8** species clearly show multiple bond characters beyond typical B=O double bonds.

As an example, we analyze in detail the OBO bonding in $LiB_2O_3^-$ (**2**). Among the MOs (Fig. S7 in the ESI†), HOMO − 7/HOMO − 8

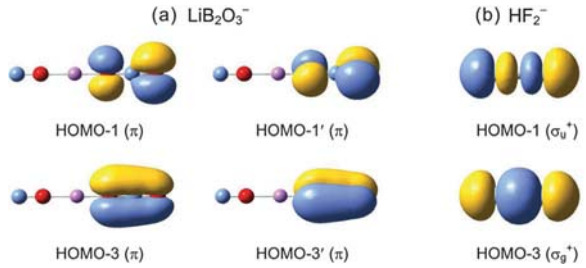

Fig. 5 (a) Dual three-center four-electron (3c-4e) π hyperbonds in $LiB_2O_3^-$ (**2**, $C_{\infty v}$, $^1\Sigma^+$), as compared to (b) the 3c-4e σ hyperbond in HF_2^- (ref. 17).

are O 2*s* lone-pairs in OBO, and HOMO − 4/HOMO − 5 are mainly responsible for the two B–O σ bonds due to the O $2p_x$ atomic orbitals (AOs). The combination of O $2p_y$ AOs results in HOMO − 3′ and HOMO − 1′, where the former is a completely bonding π MO and the latter, formally antibonding, is virtually nonbonding in nature with 33% and 59% O $2p_y$ on the two O centers, respectively (92% in total; Fig. 5a). HOMO − 3′ and HOMO − 1′ thus form a 3c-4e π hyperbond in the p_y manifold, which is reminiscent of the prototypical 3c-4e σ hyperbond (ω-bond) in XeF_2 or FHF^-.[17] The ω-bond is a type of bonding beyond the Lewis structure. In FHF^-, for example, the p_x AOs of F centers combine with the H 1*s* AO for a bonding MO and nonbonding one, both filled (Fig. 5b), where the nonbonding MO is purely F p_x AOs in nature (48% *versus* 48%). The HOMO − 3′/HOMO − 1′ 3c-4e π hyperbond in **2** is closely analogous to the ω-bond in FHF^-, except that the former is a π bond, in contrast to a σ bond in FHF^-. Concurrently, the bonding–nonbonding combination of HOMO − 3 and HOMO − 1 as another 3c-4e π hyperbond is responsible for the OBO bonding in the p_z manifold. Thus, the B center in **2** binds with both O atoms in all three directions (p_x, p_y, and p_z), collectively leading to dual 3c-4e π hyperbonds with a formally sixfold bonded B center. Dual 3c-4e hyperbonds are nonexistent in XeF_2 or FHF^-.[17] Note that OBO π bonding is highly polar in nature, which results in relatively low NRT bond orders (Tables S3–S5 in the ESI†). For example, the values are 1.80 *versus* 2.19 in **2**.

It is stressed that while a 3c-4e OBO π hyperbond is weaker than two BO single bonds, it manages to make for bonding of four electrons that would otherwise exist as two O lone-pairs. Dual 3c-4e π hyperbonds, in comparison with four O 2*p* lone-pairs, thus represent a critical bonding element in boron oxides, significantly enhancing the stability of the system. The formally sixfold bonded B center in the OBO subunit highlights its bonding capability with O. We consider the 3c-4e π hyperbonds to be the root of delocalized bonding and aromaticity in boron oxides, which may be readily extended to four-, five-, or six-membered cyclic BO rings. The latter is exemplified by the boroxol B_3O_3 ring, which dominates bulk B_2O_3 glass[42] and high-temperature liquids,[43] as well as molecular boroxine and boronyl boroxine.[11]

7. Conclusions

In conclusion, we have studied the electronic and structural properties and chemical bonding in a series of lithium and gold alloyed boron oxide clusters: $B_2O_3^-$, $LiB_2O_3^-$, $AuB_2O_3^-$, and $LiAuB_2O_3^-$. The electron affinities of B_2O_3, LiB_2O_3, AuB_2O_3, and $LiAuB_2O_3$ neutral clusters are determined *via* photoelectron spectroscopy to be 1.45 ± 0.08, 4.25 ± 0.08, 6.05 ± 0.08, and 2.40 ± 0.08 eV, respectively. Structural searches in combination with experiment allow the establishment of the global-minimum structures for these binary, ternary, and quaternary species. The $B_2O_3^-$ anion is bent, whereas the $LiB_2O_3^-$, $AuB_2O_3^-$, and $LiAuB_2O_3^-$ alloy clusters are linear or quasi-linear consisting of BO and OBO subunits. Chemical bonding in these clusters features charge transfer complexes, covalent gold, hyperhalogen, and dual three-center four-electron π hyperbonds. The concerted experimental and computational data suggest the possibility of altering and fine-tuning the properties of the boron oxide systems *via* alloying, which may result in novel, tailored electronic properties and chemical reactivities. The present approach should be applicable to other, more complicated, *n*-ary cluster and molecular systems.

Acknowledgements

This work was supported by the National Natural Science Foundation of China (No. 21243004, 21373130, and 21273246). H.J.Z. gratefully acknowledges the start-up fund from Shanxi University for support.

Notes and references

1 S. H. Bauer, *Chem. Rev.*, 1996, **96**, 1907.
2 R. J. Doyle, *J. Am. Chem. Soc.*, 1988, **110**, 4120.
3 H. Bock, L. Cederbaum, W. von Niessen, P. Paetzold, P. Rosmus and B. Soiouki, *Angew. Chem., Int. Ed. Engl.*, 1989, **28**, 88.
4 H. Braunschweig, K. Radacki and A. Schneider, *Science*, 2010, **328**, 345.
5 (*a*) H. J. Zhai, S. D. Li and L. S. Wang, *J. Am. Chem. Soc.*, 2007, **129**, 9254; (*b*) S. D. Li, H. J. Zhai and L. S. Wang, *J. Am. Chem. Soc.*, 2008, **130**, 2573; (*c*) H. J. Zhai, J. C. Guo, S. D. Li and L. S. Wang, *ChemPhysChem*, 2011, **12**, 2549.
6 D. Yu. Zubarev, A. I. Boldyrev, J. Li, H. J. Zhai and L. S. Wang, *J. Phys. Chem. A*, 2007, **111**, 1648.
7 M. L. Drummond, V. Meunier and B. G. Sumpter, *J. Phys. Chem. A*, 2007, **111**, 6539.
8 (*a*) T. B. Tai and M. T. Nguyen, *Chem. Phys. Lett.*, 2009, **483**, 35; (*b*) M. T. Nguyen, M. H. Matus, V. T. Ngan, D. J. Grant and D. A. Dixon, *J. Phys. Chem. A*, 2009, **113**, 4895; (*c*) T. B. Tai, M. T. Nguyen and D. A. Dixon, *J. Phys. Chem. A*, 2010, **114**, 2893.
9 P. G. Wenthold, J. B. Kim, K. L. Jonas and W. C. Lineberger, *J. Phys. Chem. A*, 1997, **101**, 4472.
10 H. J. Zhai, L. M. Wang, S. D. Li and L. S. Wang, *J. Phys. Chem. A*, 2007, **111**, 1030.
11 D. Z. Li, H. Bai, Q. Chen, H. G. Lu, H. J. Zhai and S. D. Li, *J. Chem. Phys.*, 2013, **138**, 244304.

12 (*a*) D. White, P. N. Walsh and D. E. Mann, *J. Chem. Phys.*, 1958, **28**, 508; (*b*) D. White, D. E. Mann, P. N. Walsh and A. Sommer, *J. Chem. Phys.*, 1960, **32**, 481; (*c*) A. Sommer, D. White, M. J. Linevsky and D. E. Mann, *J. Chem. Phys.*, 1963, **38**, 87.
13 W. Weltner, Jr. and J. R. W. Warn, *J. Chem. Phys.*, 1962, **37**, 292.
14 T. R. Burkholder and L. Andrews, *J. Chem. Phys.*, 1991, **95**, 8697.
15 P. E. Blackburn, A. Büchler and J. L. Stauffer, *J. Phys. Chem.*, 1966, **70**, 2469.
16 M. Willis, M. Gotz, A. K. Kandalam, G. F. Gantefor and P. Jena, *Angew. Chem., Int. Ed.*, 2010, **49**, 8966.
17 F. Weinhold and C. R. Landis, *Valency and Bonding: A Natural Bond Orbital Donor-Acceptor Perspective*, Cambridge University Press, Cambridge, 2005, pp. 275–306.
18 (*a*) G. L. Gutsev and A. I. Boldyrev, *Chem. Phys.*, 1981, **56**, 277; (*b*) G. L. Gutsev and A. I. Boldyrev, *Adv. Chem. Phys.*, 1985, **61**, 169.
19 P. P. Bera, K. W. Sattelmeyer, M. Saunders, H. F. Schaefer III and P. V. R. Schleyer, *J. Phys. Chem. A*, 2006, **110**, 4287.
20 (*a*) T. Krüger, *Int. J. Quantum Chem.*, 2006, **106**, 1865; (*b*) P. P. Bera, P. v. R. Schleyer and H. F. Schaefer, *Int. J. Quantum Chem.*, 2007, **107**, 2220.
21 J. M. Azpiroz, D. Moreno, A. J. M. Ugalde, M. A. Mendez-Rojas and G. Merino, *J. Mol. Model.*, 2013, **19**, 1958.
22 H. G. Xu, Z. G. Zhang, Y. Feng, J. Y. Yuan, Y. C. Zhao and W. J. Zheng, *Chem. Phys. Lett.*, 2010, **487**, 204.
23 (*a*) A. P. Sergeeva, B. B. Averkiev, H. J. Zhai, A. I. Boldyrev and L. S. Wang, *J. Chem. Phys.*, 2011, **134**, 224304; (*b*) M. Saunders, *J. Comput. Chem.*, 2004, **25**, 621.
24 D. J. Wales and J. P. K. Doye, *J. Phys. Chem. A*, 1979, **101**, 5111.
25 (*a*) C. Adamo and V. Barone, *J. Chem. Phys.*, 1998, **108**, 664; (*b*) J. P. K. Burke and Y. Wang, *Phys. Rev. B*, 1996, **54**, 16533.
26 MPW1PW91 is known to provide good results for both covalent and non-covalent interactions, which is thus a proper choice for the current clusters: (*a*) Y. Zhao, O. Tishchenko and D. G. Truhlar, *J. Phys. Chem. B*, 2005, **109**, 19046; (*b*) B. J. Lynch, P. L. Fast, M. Harris and D. G. Truhlar, *J. Phys. Chem. A*, 2000, **104**, 4811.
27 (*a*) J. Cizek, *Adv. Chem. Phys.*, 1969, **14**, 35; (*b*) G. E. Scuseria and H. F. Schaefer, *J. Chem. Phys.*, 1989, **90**, 3700; (*c*) R. J. Bartlett and M. Musial, *Rev. Mod. Phys.*, 2007, **79**, 291.
28 (*a*) W. von Niessen, J. Schirmer and L. S. Cederbaum, *Comput. Phys. Rep.*, 1984, **1**, 57; (*b*) V. G. Zakrzewski and J. V. Ortiz, *Int. J. Quantum Chem.*, 1995, **53**, 583; (*c*) J. V. Ortiz, *Adv. Quantum Chem.*, 1999, **35**, 33.
29 E. D. Glendening, J. K. Badenhoop, A. E. Reed, J. E. Carpenter, J. A. Bohmann, C. M. Morales and F. Weinhold, *NBO 5.0*, Theoretical Chemistry Institute, University of Wisconsin, Madison, 2001.
30 M. J. Frisch, *et al.*, Gaussian 09, revision D.01, Gaussian, Inc., Wallingford, CT, 2009.
31 P. G. Wenthold, D. A. Hrovat, W. T. Borden and W. C. Lineberger, *Science*, 1996, **272**, 1456.
32 Among potential isomers, the second lowest isomers, zigzag C_s (^{2}A′) $B_2O_3^-$, linear $C_{\infty v}$ ($^1\Sigma^+$) $LiB_2O_3^-$, and linear $C_{\infty v}$ ($^1\Sigma^+$) $AuB_2O_3^-$ are 0.28, 1.98, and 0.79 kcal mol^{-1} above the global-minimum structures **1–3**, respectively. Their calculated ADEs and VDEs are listed in Table S1 in ESI.† The zigzag C_s (^{2}A′) $B_2O_3^-$ and linear $C_{\infty v}$ ($^1\Sigma^+$) $AuB_2O_3^-$ generate ADEs/VDEs that are similar to **1** and **3**, hinting that they may be present experimentally as minor isomers. On the other hand, the ADE and VDE of linear $C_{\infty v}$ ($^1\Sigma^+$) $LiB_2O_3^-$ deviate substantially from experiment and can be safely ruled out.
33 D. Yu. Zubarev and A. I. Boldyrev, *Phys. Chem. Chem. Phys.*, 2008, **10**, 5207.
34 (*a*) B. Kiran, X. Li, H. J. Zhai, L. F. Cui and L. S. Wang, *Angew. Chem., Int. Ed.*, 2004, **43**, 2125; (*b*) H. J. Zhai, L. S. Wang, D. Yu. Zubarev and A. I. Boldyrev, *J. Phys. Chem. A*, 2006, **110**, 1689; (*c*) H. J. Zhai, C. Burgel, V. Bonacic-Koutecky and L. S. Wang, *J. Am. Chem. Soc.*, 2008, **130**, 9156; (*d*) X. B. Wang, Y. L. Wang, J. Yang, X. P. Xing, J. Li and L. S. Wang, *J. Am. Chem. Soc.*, 2009, **131**, 16368; (*e*) D. Yu. Zubarev, J. Li, L. S. Wang and A. I. Boldyrev, *Inorg. Chem.*, 2006, **45**, 5269.
35 J. C. Rienstra-Kiracofe, G. S. Tschumper, H. F. Schaefer III, S. Nandi and G. B. Ellison, *Chem. Rev.*, 2002, **102**, 231.
36 K. Pradhan and P. Jena, *J. Chem. Phys.*, 2011, **135**, 144305.
37 D. Samanta and P. Jena, *J. Am. Chem. Soc.*, 2012, **134**, 8400.
38 G. L. Gutsev, C. A. Weatherford, L. E. Johnson and P. Jena, *J. Comput. Chem.*, 2012, **33**, 416.
39 P. Koirala, K. Pradhan, A. K. Kandalam and P. Jena, *J. Phys. Chem. A*, 2013, **117**, 1310.
40 Y. Feng, H. G. Xu, W. J. Zheng, H. M. Zhao, A. K. Kandalam and P. Jena, *J. Chem. Phys.*, 2011, **134**, 094309.
41 P. Pyykkö and M. Atsumi, *Chem.–Eur. J.*, 2009, **15**, 12770.
42 G. Ferlat, T. Charpentier, A. P. Seitsonen, A. Takada, M. Lazzeri, L. Cormier, G. Calas and F. Mauri, *Phys. Rev. Lett.*, 2008, **101**, 065504.
43 J. D. Mackenzie, *J. Phys. Chem.*, 1959, **63**, 1875.

